

This work was written as part of one of the author's official duties as an Employee of the United States Government and is therefore a work of the United States Government. In accordance with 17 U.S.C. 105, no copyright protection is available for such works under U.S. Law.

Public Domain Mark 1.0

<https://creativecommons.org/publicdomain/mark/1.0/>

Access to this work was provided by the University of Maryland, Baltimore County (UMBC) ScholarWorks@UMBC digital repository on the Maryland Shared Open Access (MD-SOAR) platform.

Please provide feedback

Please support the ScholarWorks@UMBC repository by emailing scholarworks-group@umbc.edu and telling us what having access to this work means to you and why it's important to you. Thank you.

Cluster observations near reconnection X lines in Earth's magnetotail current sheet

K.-J. Hwang,^{1,2} M. L. Goldstein,¹ D. E. Wendel,¹ A. N. Fazakerley,³ and C. Gurgiolo⁴

Received 15 February 2013; revised 10 May 2013; accepted 16 June 2013; published 19 July 2013.

[1] Magnetic reconnection is an efficient way to convert magnetic energy into particle energy. In this paper, we use Cluster thermal electron and ion measurements in the vicinity of a reconnection X line to delineate the structure of the reconnection current sheet. Multispacecraft observations made by Cluster on 18 August 2002 indicate that an X line drifted close to the spacecraft, about $3.4 R_E$ earthward of the position where another X line had been observed earlier. Comparison of the Hall magnetic and electric field geometry and the observed properties of energetic electron beams streaming along the separatrix between the Cluster spacecraft indicates that the second X line formed within 20 s of the observation of the first X line. Repeated flow reversals and Hall field geometry together with the presence of a magnetic island embedded in the outflow region downstream of the first X line suggest that the initial current sheet was unstable, perhaps to the tearing mode. We identify a region with a thickness of 0.72 ion inertial lengths (29 electron inertial lengths, d_e) of super-Alfvénic electron outflow (greater than the ion in-flow Alfvén speed) during the period when the spacecraft was in the vicinity of the neutral sheet. Slightly below the neutral sheet, Cluster observed asymmetric counter-streaming electrons with a loss of axisymmetry in the electron ($V_{\perp 1}, V_{\perp 2}$) distribution functions over a thin boundary with a thickness of several d_e . This electron-scale transition layer was embedded in a much wider region where both the ion and electron Walén tests failed, and the electron super-Alfvénic bulk outflow jets with high-energy electron beams were detected. Those phenomena provide details of the substructure of the reconnection current sheet and suggest that the spacecraft traversed or skimmed the tailward edge of an elongated electron current layer. We also note that this event differs from a previously reported reconnection event in that strong electron temperature anisotropy ($T_{\parallel} > T_{\perp}$) is observed both in the inflow region and in the exhaust, where the anisotropy appears to be associated with the elongated electron outflow jets.

Citation: Hwang, K.-J., M. L. Goldstein, D. E. Wendel, A. N. Fazakerley, and C. Gurgiolo (2013), Cluster observations near reconnection X lines in Earth's magnetotail current sheet, *J. Geophys. Res. Space Physics*, 118, 4199–4209, doi:10.1002/jgra.50403.

1. Introduction

[2] Magnetic reconnection converts magnetic energy into particle energy—often rapidly and efficiently, such as in solar flares and magnetospheric substorms. The multiscale nature of reconnection has long been a focus of study in both space and laboratory plasmas. The initiation and reconfiguration of magnetic topology associated with reconnection are thought to arise as a result of demagnetization of

electrons within the small electron diffusion region (EDR). This region is embedded within a much larger ion diffusion region (IDR) where ions are demagnetized. Although IDRs, where Hall physics governs the magnetofluid description, have been identified by their magnetic and electric field geometry [Wygant *et al.*, 2005; Vaivads *et al.*, 2006; Eastwood *et al.*, 2010], the electron diffusion region is difficult to observe primarily because of its small-scale size coupled with the generally long cadences associated with plasma measurements.

[3] Previous numerical studies by Shay *et al.* [1999], Birn *et al.* [2001], Hesse *et al.* [1999], and Ricci *et al.* [2002] showed that the reconnection rate in the regime of quasi-steady reconnection is insensitive to the dynamics occurring on the scale of the EDR. In contrast, Karimabadi *et al.* [2007] have suggested that frequent formation of plasmoids resulting from instabilities excited in elongated EDRs can lead to significant variations in the reconnection rate. Numerous studies using full particle-in-cell (PIC)

¹NASA Goddard Space Flight Center, Greenbelt, Maryland, USA.

²The Goddard Planetary Heliophysics Institute, University of Maryland, Baltimore County, Baltimore, Maryland, USA.

³Mullard Space Science Laboratory, University College London, Dorking, UK.

⁴Bitterroot Basic Research, Hamilton, Montana, USA.

Corresponding author: K.-J. Hwang, NASA Goddard Space Flight Center, Greenbelt, MD 20771, USA. (kyoung-joo.hwang@nasa.gov)

©2013. American Geophysical Union. All Rights Reserved.
2169-9380/13/10.1002/jgra.50403

simulations [Cai and Lee, 1997; Horiuchi and Sato, 1997; Pritchett, 2002; Hesse et al., 2004; Scudder and Daughton, 2008] have been performed to investigate the relative roles of nongyrotropic electron pressure and electron inertia in balancing the reconnection electric field. The consensus is that nongyrotropic pressure forces dominate over electron inertial force. Hesse et al. [2004] and Hesse [2006], using PIC simulations, showed that the nongyrotropic electron distribution can form from a mixture of high-velocity particles leaving the EDR with a population of lower velocity electrons entering it. This situation arises from the strong gradient of the parallel electric field across the electron current layer. Hesse [2006] proposed that a nongyrotropic pressure tensor would produce effective parallel heating and maintain the current density in the EDR, even in the presence of a guide field.

[4] Several papers have endeavored to identify the EDR using both observations and/or numerical simulations. Scudder et al. [2002] suggested that nonzero parallel electric fields supported by an electron pressure force on the scale of $\beta^{\frac{1}{2}} c/\omega_{pe}$, together with simultaneous observations of a super-Alfvénic parallel electron bulk flow are signatures of being within the EDR. One diagnostic of being within an EDR proposed by Mozer et al. [2005] is a combination of a nonzero parallel electric field over a scale size of an electron inertial length (c/ω_{pe}), a perpendicular electric field that exceeds the reconnection electric field, large Joule dissipation, acceleration of an electron beam, and a change of magnetic topology (as identified by the $\mathbf{E} \times \mathbf{B}/B^2$ flow). In the Earth's magnetotail, Phan et al. [2007] identified an elongated EDR of $\sim 60 c/\omega_{pi}$ from the observation of a super-Alfvénic electron outflow jet along the current sheet (also see Shay et al. [2007]). Scudder and Daughton [2008] suggested that the nongyrotropy of the electron pressure tensor is an indicator of the EDR for either X or O lines of the neutral sheet geometry. Recently, Scudder et al. [2012] have used data from the Polar spacecraft to identify an EDR at the Earth's magnetopause.

[5] Although the EDR is, in general, difficult to identify solely using electron distribution functions obtained with relatively long cadences (here 4 s), electron distribution functions can delineate the substructure of the current sheet where reconnection is occurring. Chen et al. [2008b] and Wang et al. [2011] used the observations of temperature anisotropy and variations in electron moments to identify magnetic islands and the scale sizes of an electron current layer.

[6] The anisotropic electron pressure with $p_{\parallel} > p_{\perp}$ within the reconnection region was first reported by Øieroset et al. [2002]. This anisotropy was subsequently accounted for in a numerical study by Egedal et al. [2005]. It was found that the cause of the anisotropy is electron trapping by magnetic mirror forces and parallel electric fields. An analytical form of the electron distribution function accounting for the anisotropy was derived in Egedal et al. [2008] and successfully compared [Egedal et al., 2010] to the anisotropic electron distributions observed by the Cluster mission in the 1 October 2001 event [Chen et al., 2008a]. Le et al. [2009] derived new fluid-closure equations to describe the state functions (p_{\parallel} and p_{\perp}) for magnetized electrons in a collisionless regime. They found that the trapping of electrons accurately treats the pressure anisotropy. In subsequent fluid

simulations using the new fluid closure, it was demonstrated that the pressure anisotropy can drive large-scale elongated electron current layers within the reconnection region [Ohia et al., 2012].

[7] In this paper, we use data from Cluster to present an unusual observation of multiple ion-scale Hall structures in the Earth's magnetotail current sheet. The observations suggest that the spacecraft passed near a current sheet that was likely unstable to the tearing instability. There were two near-X line encounters within a 20 s time frame which provides important clues about the structure of reconnection layers and how X lines develop and evolve. We describe several detailed features of the electron distribution functions along the spacecraft trajectory across the current sheet. In particular, we report that near a reconnection X line, there is a unique signature in the electron distribution function associated with traversing a sharp boundary in the electron current sheet. We describe the electric and magnetic fields, as well as electron distributions and associated outflow jets, in the vicinity of the EDR. We point out that this event exhibits significant differences from the reconnection event analyzed in Chen et al. [2008a, 2009a] where strong electron temperature anisotropy with $T_{\parallel} > T_{\perp}$ was observed in the inflow regions, whereas the electron distributions in the exhaust were nearly isotropic. In contrast, for the present reconnection event, strong anisotropy is also observed in the exhaust and appears to be associated with the large-scale, elongated region of electron outflowing jets. This observation is consistent with a recent numerical study by Le et al. [2013], who showed that the temperature anisotropy develops by electron trapping in the reconnection inflow and extends to the exhaust if the guide field is sufficiently strong so as to maintain the electrons to be magnetized.

[8] In section 2 we describe the overview of the event that suggests a multiple near-X line geometry along the magnetotail axis with a plasmoid embedded in the outflow region where the bulk velocity of outflowing electrons is greater than the inflow Alfvén speed. In section 3 we present electron distribution functions at locations along the spacecraft trajectory to delineate the substructure of the current sheet where reconnection is occurring. Section 4 summarizes our observational results.

2. Multiple Near-X Line Structures

[9] On 18 August 2002, the Cluster spacecraft crossed the central current sheet at approximately $(-17.4, -6.0, -1.6)$ Earth radii (R_E) in GSM coordinates. This event is illustrated in Figure 1A(a–f). Shown are the magnetic and electric field components and the ion flow velocity from both C4 (a–c) and C1 (d–f). Data are given in the current sheet coordinate system denoted by $[l, m, n]$ where \hat{l} is parallel to the current sheet, \hat{n} is normal to the current sheet, and $\hat{m} = \hat{n} \times \hat{l}$ (Figure 1B). The directions are derived from a minimum variance analysis during the period of the current sheet traversal that occurs between the two dashed vertical orange lines. The two spacecraft are separated at this time by ~ 3504 km, mainly along \hat{l} .

[10] The event includes two tailward to earthward flow reversals. The first flow reversal occurs between the two dashed green lines and the second within the time interval delineated by the two dashed cyan lines. The current sheet

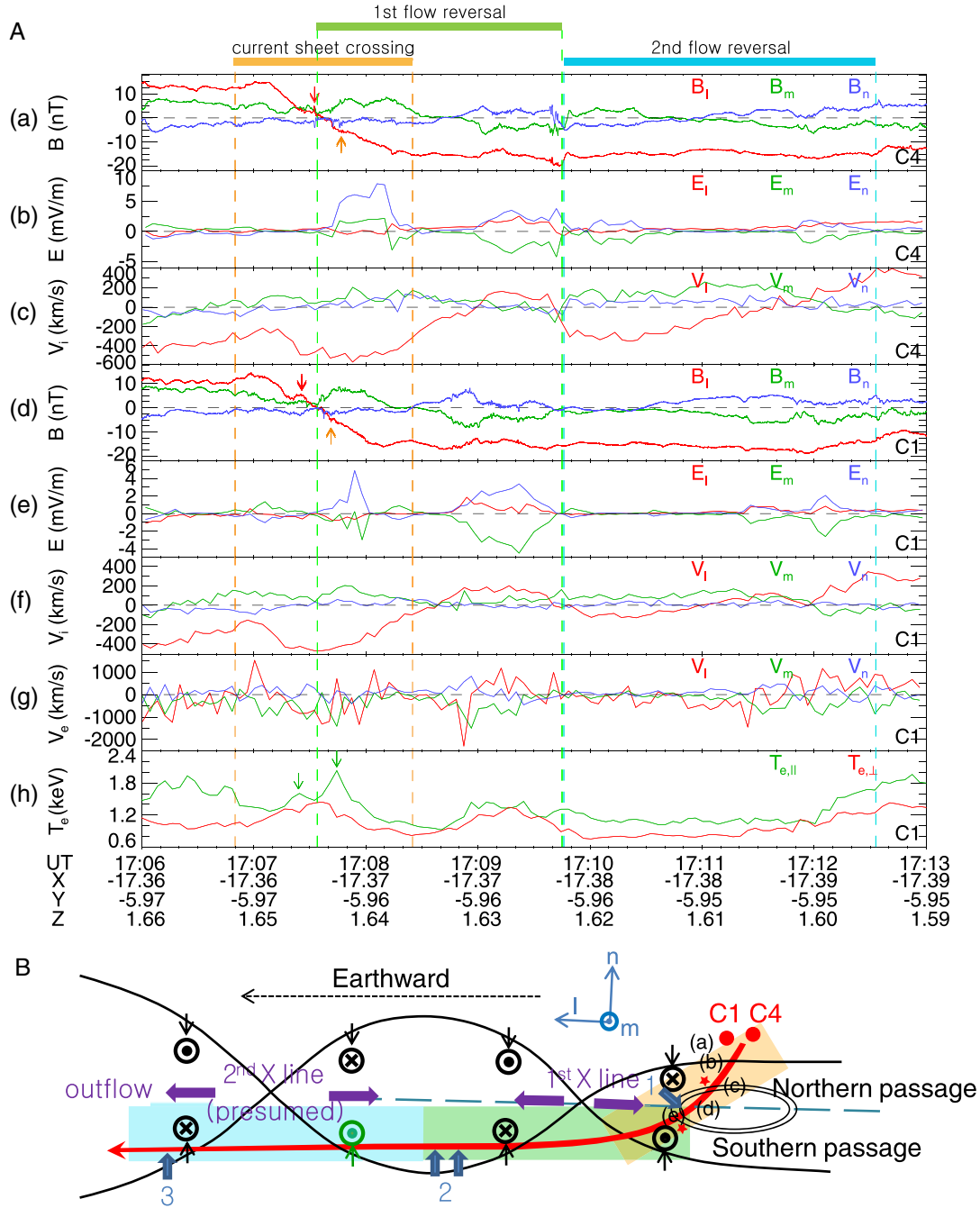


Figure 1. (A) C4 (a–c) and C1 (d–j) data in the current-sheet coordinates: magnetic field (a, d), B_i (red), B_m (green), and B_n (blue); electric field (b, e), E_i (red), E_m (green), and E_n (blue); ion (c, f) and electron (g) velocity, V_i (red), and V_m (green), V_n (blue); electron parallel (green) and perpendicular (red) temperature (h). (B) The relative trajectory of C1/4 across the multiple X line structures. Orange, green, and blue shades depict the current sheet crossing, the first, and the second flow reversal, respectively. Red stars indicate a possible northern and southern traversal of the plasmoid structure embedded in the outflow region, associated with a transient enhancement of B_i , marked by red and orange arrows in Figure 1A(a, d) and electron temperature anisotropy $[T_{\parallel} > T_{\perp}]$, green arrows in Figure 1A(d). During the second flow reversal (blue-shaded region), C1 did not observe tailwardside Hall fields (denoted by green symbols), although such fields were observed by C4 later. Blue arrows with numbers 1–3 corresponding to those in Figures 2b and 2c delineate where energetic electron fluxes are found. The locations (a–e) where electron distributions are sampled in Figure 4.

crossing from north to south occurs near 1707:33 UT in both C4 and C1 as indicated by the change in sign in B_l (positive to negative). Various aspects of the current sheet traversal and the first flow reversal have already been described in *Åsnes et al.* [2008]. The first reversal of the bulk plasma flow from tailward to earthward (negative V_l to positive V_l) occurs at $\sim 1709:00$ UT in C4 and $\sim 1708:40$ UT in C1. Flow reversals observed by both C1 and C4 are accompanied by bipolar changes (positive to negative) in B_m and a pair of positive E_n , which primarily represent the Hall magnetic geometry. The second flow reversal occurs at $\sim 1711:00$ UT on C1 and $\sim 1711:35$ UT on C4. Only C4, which detected the more prominent flow reversal, observes bipolar changes in B_m and a pair of positive E_n around the flow reversal time (detailed below).

[11] The average magnetic field ($\langle \mathbf{B}_m \rangle$) prior to the first flow reversal is about 6 nT, which represents a “guide field” component (B_{guide}). The negative-to-positive variations in both $\delta B_m (B_m - B_{\text{guide}})$ and E_n across the first dashed green vertical line in Figure 1A (most clearly seen in d and e), together with a tailward bulk flow during these field variations are consistent with a north to south passage through a current sheet tailward of an X line (the orange-shaded region in Figure 1B). Note the short increase in B_l (red arrows in a and d of Figure 1A) before C1 and C4 traverse the magnetic field minimum.

[12] The timing of the increase in B_l almost corresponds to transient enhancements in the electron temperature anisotropy ($T_{\parallel} > T_{\perp}$) seen in h of Figure 1A (the first green arrow). There is another peak in the electron temperature anisotropy (the second green arrow in h) that is symmetric about the current sheet crossing at $\sim 1707:33$ UT, observed immediately below the current sheet. Within the time between the two peaks in the electron temperature anisotropy associated with the spike in B_l , there is an enhancement in the high-energy electron fluxes in the RAPID data (in Figures 2b and 2c). These observations imply that the short increase in magnetic strength (B_l) represents a magnetic island or plasmoid structure embedded in the current sheet [*Eastwood et al.*, 2007; *Chen et al.*, 2009b; *Wang et al.*, 2011], rather than arising from magnetic pileup within the outflow region of the reconnection site where the increase of B_n will be most prominent and T_{\perp} is generally expected to be greater than T_{\parallel} due to betatron acceleration, and/or nonadiabatic curvature and $\nabla \mathbf{B}$ drifts [*Hoshino et al.*, 2001; *Hoshino*, 2005].

[13] A superposed epoch analysis of the instantaneous field structure around the current sheet [*Wendel and Reiff*, 2009] for this event also indicates an O line or plasmoid neutral sheet geometry (not shown). The magnetic gradients along \hat{l} and \hat{n} support this interpretation. The other expected pair of increases in magnetic strength on the southern side of the center of the plasmoid (orange arrows in a and d of Figure 1A) are not as clear as are the first pair (red arrows). Observing such increases, however, depends sensitively on the spacecraft trajectory (see Figure 1B, which illustrates a possible Cluster trajectory that crosses the northern and southern side of the plasmoid indicated by red stars). Nonetheless, the second peak in T_{\parallel} (at $\sim 1707:43$ UT) in h of Figure 1A implies the existence of a plasmoid. This region is found to be coincident with an elongated electron current layer embedded in the exhaust (to be described in

the following section). Recent simulations suggest that an instability in an elongated electron current sheet can cause the layer to be disrupted, e.g., leading to frequent formation of plasmoids [*Karimabadi et al.*, 2007]. The theoretical idea that the temperature anisotropy is caused by electron trapping [*Egedal et al.*, 2005, 2008, 2010; *Le et al.*, 2009; *Ohia et al.*, 2012] suggests that the current layer is unstable to an instability such as a firehose that disrupts the layer, causing it to become more filamentary and/or bifurcated. This evolution can explain the observation of the second peak in T_{\parallel} .

[14] Positive-to-negative changes in B_m with positive E_n components on both sides of the first flow reversal (bounded by two green dashed vertical lines in Figure 1A) signify Hall fields around a reconnection X line along the earthward trajectories of C1 and C4 relative to the structure (see Figure 1B). Also, negative-to-positive B_n variations during the first flow reversal suggest an X-shaped geometry on the southern side of the X line. Note that the times of the flow reversal in the frame of the X line, which drifts along negative \hat{l} at ~ 175 km/s and along positive \hat{n} at ~ 17 km/s as estimated from a two-spacecraft timing analysis, are consistent with the timings of the reversal of B_m and E_n .

[15] During the second flow reversal, only C4 observed Hall magnetic and electric fields on both sides of the X line. The field and flow reversals at C4 are similar to those seen during the first flow reversal. The implication here is that a second X line structure has passed above the spacecraft and about $3.4 R_E$ earthward of the first X line. This interpretation assumes that the entire structure of the two X lines moved at a velocity of ~ 175 km/s in the negative \hat{l} direction. On the other hand, the Hall magnetic and electric fields observed by C1 appear only on the earthward side Hall region of the second X line, i.e., thus C1 did not observe the tailward portion of the quadrupolar Hall signatures (denoted by the green symbol and arrow in Figure 1B).

[16] During the second flow reversal, differences in the high-energy electrons as seen on C1 and C4 help to constrain the spatial and/or dynamic properties of the event. Blue arrows in the time series in Figures 2b and 2c and in the cartoon in Figure 1B denote the times when high-energy electron fluxes (up to above 100 keV) are enhanced. The enhancement at label “2” is very pronounced and occurs in the earthward side and southern side of the Hall region. C1 detects enhancements of primarily tailward fluxes with some earthward fluxes as shown in the pitch angle distribution of the electron fluxes (Figure 2e), while C4 mainly sees bidirectional (one close to be parallel and the other close to be antiparallel to the magnetic field) high-energy electron fluxes. These bidirectional fluxes are observed until C4 traverses the second flow reversal at $\sim 1711:00$ UT. Similar high-energy fluxes have been found in association with X line crossings by *Phan et al.* [2007]. It seems plausible that the bidirectional beams seen on C4 originate at the two reconnection sites, one earthward and the other tailward of the observation location. We also note that the enhanced high-energy electron fluxes around “2,” compared to “1” are neither exactly parallel nor antiparallel to the local magnetic field, but rather form a conic or butterfly-like distribution (Figures 2e and 2g), which implies pitch angle changes of the energetic electrons associated with changes

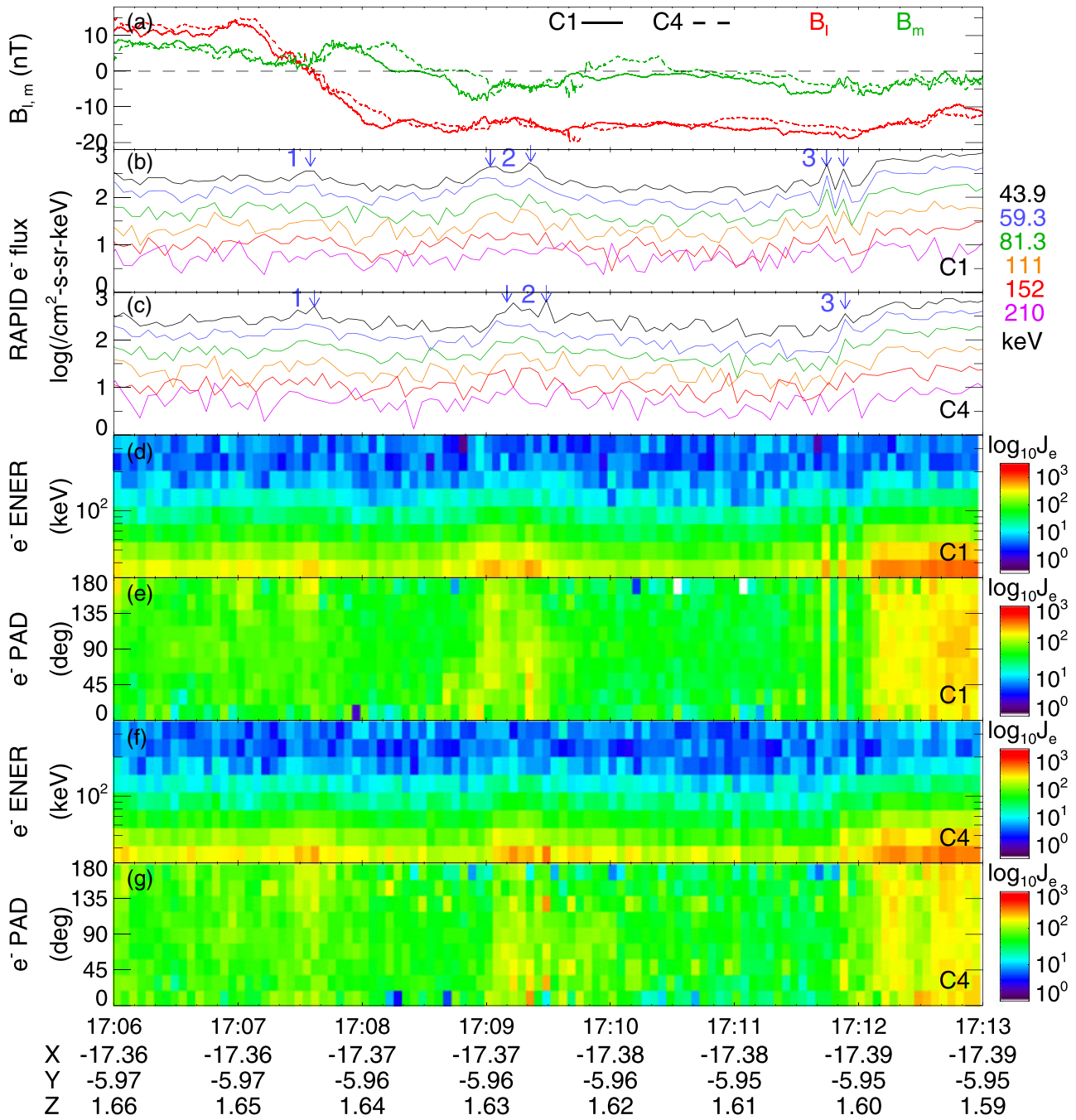


Figure 2. High-energy electron features during the event observed by C1 and C4 from RAPID: (a) the magnetic field components as a reference of the structure, (b, c) electron differential fluxes at the central energies, 43.9, 59.3, 81.3, 111, 152, and 210 keV, (d, f) the energy spectrogram, and (e, g) the pitch angle distribution.

in the magnetic field strength, which is larger and away from the X line.

[17] Although the previous scenario can be interpreted in terms of stationary structures passing the spacecraft, we feel that a dynamic scenario better fits the observed differences seen at C1 and C4. We suggest that the second X line developed during the ~ 20 s interval between the passage of C1 and C4 through the same region. The development of the second X line accounts naturally for the fact that C1 detected mainly tailward high-energy electron beams that originated

from the reconnection site around the second X line, rather than earthward beams that originated from the reconnection site around the first X line. The high-energy electron beams would have contributed to the electric current in the EDR as the second X line developed. This interpretation implies that C1 observed an early-phase signature of the new X line, i.e., high-energy electron beams leaving the newly formed X line, but then missed the tailwardside Hall structure that formed later. C1 did, however, observe its earthward-side Hall structure. This scenario incorporates the idea that

magnetic reconnection starts in the EDR with the production of high-energy electrons.

[18] The entire structure, i.e., the O line geometry observed during the current sheet crossing and consecutive Hall field observations during the two flow reversals, points to the presence of a quasiperiodic reconnection geometry along the magnetotail current sheet. Such a geometry could well result from excitation of the tearing-mode instability. To test whether or not the criteria for the instability were met [Furth *et al.*, 1963; Coppi *et al.*, 1966], we assume that the separation of the two X lines along \hat{l} is an estimate of the wavelength of the initial mode. The thickness of the current sheet was estimated (1) from the spacecraft separation along \hat{n} and also (2) by fitting the four-point magnetic field variations taken prior to detection of the first tailward flow (at ~ 1700 UT) to a Harris model. During this event, C2, located about $0.47 R_E$ duskward of the other spacecraft barely observed the current sheet, while C3, located about $0.47 R_E$ below C1 and C4 in the Southern Hemisphere was below the current sheet and completely missed the structures seen by C1 and C4. Consequently, the thickness of the initial current sheet (Δ) was less than the current sheet normal separation of C3 to the other spacecraft ($\Delta \leq 0.47 R_E$). The Harris sheet model yields $\Delta \approx 0.44 R_E$. Both estimates of Δ satisfy $k\Delta (= 0.81 - 0.87) \leq 1$ [Furth *et al.*, 1963; Coppi *et al.*, 1966], where k is the wave number associated with the spacing along \hat{l} of the inferred tearing-mode structure, i.e., the separation of the two X lines along \hat{l} . Therefore, we conclude that the magnetotail current sheet prior to and/or during this event could well have been unstable to the tearing instability. Although we cannot investigate the small-scale dynamics of the instability, the appearance of a plasmoid coinciding with the electron super-Alfvénic outflowing jet (section 3) suggests that an instability in the elongated electron current sheet might have caused the plasmoid to form [Karimabadi *et al.*, 2007].

3. The Substructure of the Reconnection Current Sheet Layer

[19] During the current sheet crossing (1706:50–1708:25 UT), the spacecraft were closest to the magnetic X line. Between 1707:00 and 1708:04 UT, the data show super-Alfvénic electrons moving at a speed larger than $V_{A, \text{inflow}}$ in the frame of the X line [Figure 1A(f–g)] ($V_{A, \text{inflow}} = B/\sqrt{\mu_0 \rho}$ is the inflow Alfvén speed, B is the ambient magnetic field, and ρ is the plasma mass density in the inflow region; $V_{A, \text{inflow}} \sim 500$ km/s prior to the current sheet crossing). The largest electron super-Alfvénic jet at 1707:00–04 UT and 1707:36–44 UT seemed to occur when C1 crossed the separatrix and passed close to the neutral sheet region, respectively. The scale size of the super-Alfvénic outflow layer along \hat{l} downstream of the X line (using the estimated X line velocity and reconnection geometry [Phan *et al.*, 2007]) is 53 ion inertial lengths ($d_i \sim 500$ km). Its width along \hat{n} is about $0.72 d_i$ or $29 d_e$ (d_e is the electron inertial length, ~ 12 km). The values are compared to those reported by Phan *et al.* [2007], who found an elongated EDR of an electron super-Alfvénic jet that covered ~ 63 ion inertial lengths along the current sheet and 9 electron inertial lengths normal to the current layer. The event described here, therefore, has a thicker layer of an outflow jet of super-Alfvénic

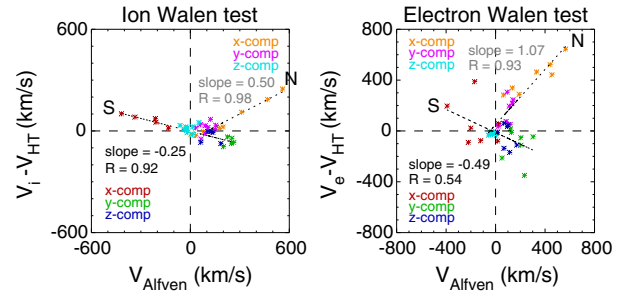


Figure 3. (left) Ion and (right) electron Walén tests for the northern (denoted by “N”) and southern (S) passages of the current sheet, denoted by an orange shade in Figure 1.

electrons than seen by Phan *et al.* [2007]. The difference is likely associated with the formation of the magnetic island (described in section 2) in the outflow region that prevented the current sheet from extending and thinning. Karimabadi *et al.* [2007] proposed that frequent formation of plasmoids from instabilities in the elongated EDR can affect the reconnection rate. Recently, Ohia *et al.* [2012] and Le *et al.* [2013] demonstrated that electron pressure anisotropy that develops in the exhaust region (to be described below and shown in Figure 4) can support the extended electron current layer.

[20] The observation that the electron outflow speed is not bounded by the inflow Alfvén speed is expected from both analytic analysis and from numerical simulations [Shay *et al.*, 1999] as a consequence of the quadratic property of the dispersion relation of whistler waves that are thought to control the physics in the ion diffusion region. The large electron bulk velocity helps to sustain most of the electric current density in the dissipation region where $\mathbf{J} \cdot \mathbf{E} > 0$ [Hesse, 2006]. Because the current \mathbf{J} is carried primarily by electrons in the EDR, the observation of the large electron velocity might also suggest a proximity to the EDR [Phan *et al.*, 2007; Scudder *et al.*, 2012].

[21] To further explore the reconnection substructure, we performed a Walén test in the deHoffmann-Teller frame separately for ions [Chanteur, 1998] and electrons. The Walén test locates rotational discontinuities that describe the current sheet layer under ongoing reconnection. For electrons, we used the generalized Walén relation formula, adopted from equation (32) of Scudder *et al.* [1999] that takes into account the electron pressure anisotropy. For the northern passage, before C1 crosses the neutral sheet (denoted by “N” in Figure 3), only the electron Walén test shows a slope of close to 1, as would be expected between jumps across an ongoing reconnection boundary (i.e., a rotational discontinuity). The ions for the same time period show a slope of 0.5. During the southern passage below the neutral sheet (S), neither the ions nor electrons satisfy the Walén test (the slopes are < 1). In fact, the electrons do not show any significant correlation (right panel in Figure 3) between $(V_e - V_{HT})$ and $V_{Alfvén}$. This suggests that north of the neutral sheet the spacecraft was mostly in the IDR where electrons were still magnetized, while on the southern passage of the current sheet, the spacecraft passed at least close to the EDR where both ions and electrons are demagnetized. (The spacecraft trajectory relative to the reconnection geometry shown in Figure 1B depicts the proximity to the X line during Cluster’s southern passage of the current sheet.)

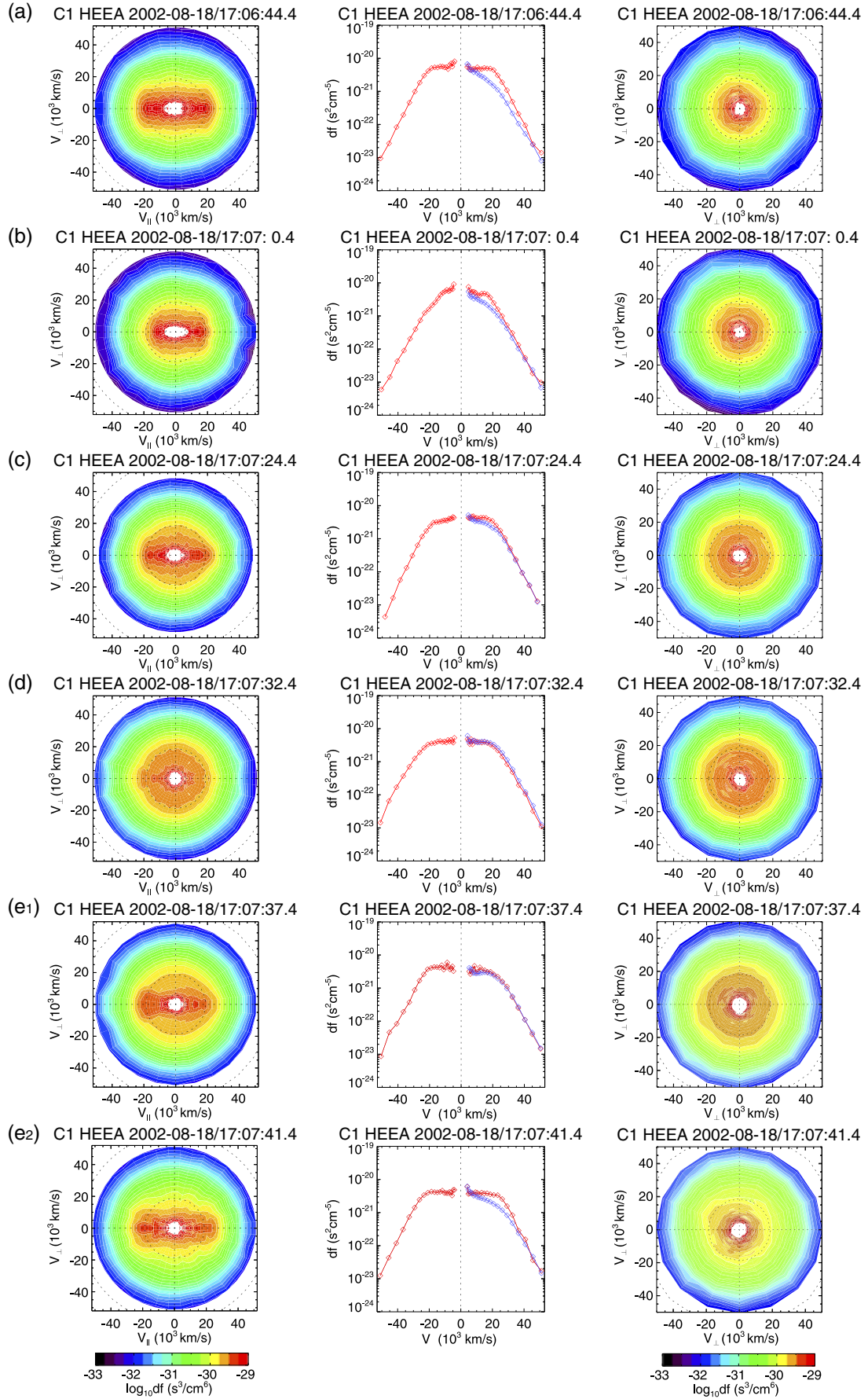


Figure 4

[22] Motivated by this observation, we examined whether or not we could delineate the substructure of the reconnection current sheet layer by looking in detail at the electron distribution functions along the C1 trajectory. Figure 4 shows a selected set of distributions along the orbit starting in the inflow region (Figure 4a), then the separatrix region (Figure 4b), plasmoid (Figure 4c), and entry into the neutral sheet (Figure 4d) followed by distributions acquired immediately below the neutral sheet (e_1 and e_2), including the time of the intense super-Alfvénic flows. All distribution plots have a $\sim 19 \times 10^3$ km/s circle corresponding to electron energies of 1 keV overlaid on them to make comparisons between plots easier. The times above each plot are center times for the 3-D distributions to be sampled (4 s). The left column of plots of Figure 4 shows the electron distributions as a function of $(V_{\parallel}, V_{\perp})$ while the right column shows the distribution as a function of $(V_{\perp 1}, V_{\perp 2})$. (Parallel and perpendicular are defined with respect to magnetic field direction, which does not exhibit significant variations within the 4 s intervals represented in the plots.) The middle column of Figure 4 displays line plots of the reduced distribution functions obtained by integrating $f(V_{\parallel}, V_{\perp})$ over V_{\perp} (red trace; f_{\parallel}) and V_{\parallel} (blue trace; f_{\perp}).

[23] Figure 4a shows details typical of the electron distribution functions in the inflow region (the relative location can be seen in Figure 1B(a)). The distribution consists basically of a core electron distribution together with a pair of counter-streaming beams that largely account for the apparent temperature anisotropy, $T_{\parallel} > T_{\perp}$. The counter-streaming beams (in the $+$ and $-x$ directions) are symmetric in that the magnitude of the bulk drift velocity, beam density, and the thermal spread are comparable. The symmetry suggests that as the electrons move toward the diffusion region, they undergo reflection either off a potential boundary or at a mirror point surrounding a region of weak magnetic field. *Egedal et al.* [2005, 2008, 2013] showed that the temperature anisotropy develops when electrons trapped in this fashion encounter a continued decrease in magnetic strength, which causes their perpendicular energy to decrease as required to conserve their magnetic moments. The positive slope ($\frac{df_{\parallel}}{dV_{\parallel}} > 0$) near the beam distributions (often observed in the inflow region in this event and glimpsed in the middle plot of Figure 4a) provides a free energy source for the generation of waves and instabilities that may further heat the beams. Indeed, Cluster observed broadband electrostatic wave enhancements (not shown) that extended far above the electron cyclotron frequency during passage through the inflow region.

[24] The separatrix region (Figure 4b) is also characterized by a pair of counter-streaming electron beams that are not quite as symmetric as those in the inflow region. The difference in electron fluxes into and out of an X line along the separatrices, or reflection of a portion of the initial electron beam flowing into an X line, can cause such asymmetry between the two beams, as can temporal variations which occur within the 2 s separating the beam measurements. The beams are neither as intense nor as fast at those seen in the inflow region. This can be seen by comparing them to the dotted 1 keV circle.

[25] Figure 4c shows electron distributions centered at 1707:24 UT during which time C1 crossed the northern hemispheric saddle point of the magnetic island downstream of the X line (Figure 1B(c)). The overall distributions for both $(V_{\parallel}, V_{\perp})$ and $(V_{\perp 1}, V_{\perp 2})$ plots are very similar to those observed during the neutral sheet crossing (Figure 4d) except for the presence of the superposed parallel and antiparallel beams. These electron beams are populations that drift along the plasmoid magnetic field (described in section 2) and contribute to the apparent temperature anisotropy. The structure of the $(V_{\parallel}, V_{\perp})$ distributions implies successive emergence of beams that have differential drift speeds, which indicates either the introduction of a new population or the presence of an evolving plasmoid or magnetic island. The increase in the overall perpendicular temperature is an indicator of the nearness of the spacecraft to the neutral sheet (Figure 1A(h)).

[26] Near the neutral sheet (Figure 4d) closest to the magnetic null, or O line (Figure 1B(d)), the electron distribution is isotropic with a flat top and a higher temperature, perhaps a consequence of kinetic dissipation occurring within the neutral sheet. Figures 4e₁ and 4e₂ correspond to two consecutive spins of data that were obtained just below the neutral sheet (Figure 1B(e)) within the time period when the electron Walén relation failed in Figure 3 and when the fastest electron super-Alfvénic jet ($\sim 3V_{A, \text{inflow}}$) was detected. The electron distributions show counter-streaming beams that appear more isolated from the core populations than at other locations. The beams are asymmetric in density, drift velocity, and temperature between the two counter-streaming components (compare two shoulders of f_{\parallel} in the middle panel of Figure 4e₁).

[27] The axisymmetry shown in the $f(V_{\perp 1}, V_{\perp 2})$ plots (the right column of Figure 4) for regions (a–e) (see Figure 1B(a–e)) indicates that the distributions are, in general, gyrotropic for these regions. Around 1707:39 UT, there is a noticeable change in the electron distribution from 1707:37 UT to 1707:41 UT (Figures 4e₁ and 4e₂) which

Figure 4. The electron distribution functions at the time of crossing (a) the inflow region at $\sim 1706:44$ UT, (b) a separatrix at $\sim 1707:00$ UT, (c) the northern hemispheric boundary of a magnetic island downstream of the X line at $\sim 1707:24$ UT, (d) the neutral sheet with a minimum of magnetic strength at $\sim 1707:32$ UT, and (e₁ and e₂) slightly below the neutral sheet at $\sim 1707:40$ UT. The left column shows the electron distributions as a function of $(V_{\parallel}, V_{\perp})$, the middle one shows the reduced distribution functions along the direction parallel (red) and perpendicular (blue) to the local magnetic field, and the right one shows the distributions as a function of $(V_{\perp 1}, V_{\perp 2})$ from the 3-D electron distributions. Corresponding locations where in the current sheet frame the electron distributions are sampled are denoted along the spacecraft trajectory in Figure 1B(a–e). Inner (outer) dashed circles overlaid in all 2-D distribution plots correspond to velocities of electron energies of 1 (10) keV.

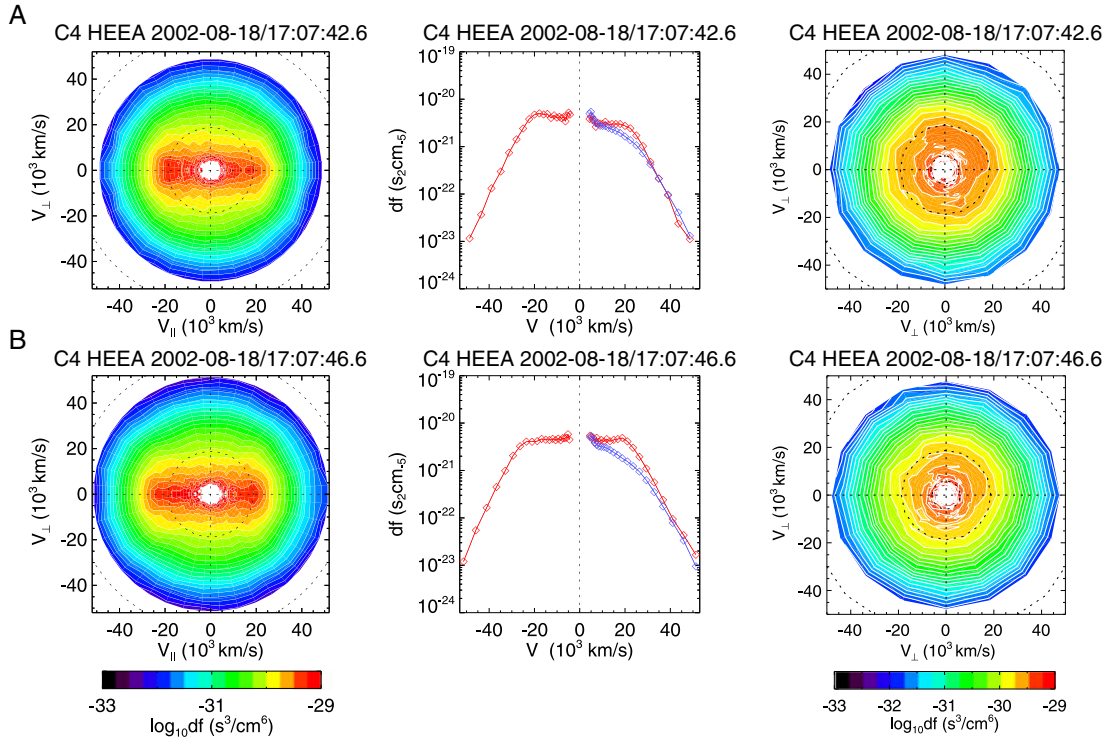


Figure 5. Same format as Figure 4, but from C4 observations during the crossing of a transition layer.

consists of the absence of an almost isotropic low-energy population (compare orange-yellow contours in the left panels of Figures 4e₁ and 4e₂) together with a noticeable cooling of the core electron population in the $f(V_{\perp 1}, V_{\perp 2})$ plots. This change probably represents a sharp boundary crossing. However, this boundary signature is primarily seen in the electron distributions (Figures 4e₁ and 4e₂) and barely identifiable in other physical quantities, such as the magnetic field, plasma density, and bulk flow. *Le et al.* [2013] attributed similar changes in the electron distribution functions in their numerical study to a transfer of some of the parallel heating of the bidirectional distribution into perpendicular directions when weak pitch angle diffusion is present in the exhaust. They suggested that such pitch angle diffusion can be caused by regions of the low magnetic field magnitude where the electrons become unmagnetized, or by instabilities including the electron firehose instability.

[28] When C4 crossed the same region in ~ 6 s later, a similar, but more gradual change in the electron distribution function was detected between 1707:40.6 and 48.6 UT. During this period C4 detected electron super-Alfvénic jets and the $(V_{\perp 1}, V_{\perp 2})$ distributions showed a loss of axisymmetry. The rightmost column of Figure 5 shows two consecutive spins of $f(V_{\perp 1}, V_{\perp 2})$ from C4. The leftmost column of Figure 5, $f(V_{\parallel}, V_{\perp})$ shows that antiparallel/parallel beam properties are varying rapidly during the transition. The asymmetric counter-streaming electron populations are predicted from simulations to exist in the EDR and are attributed to the mixing between parallel and antiparallel components that have different acceleration histories over a region of rapidly varying fields with distance and/or result from electron trapping by the potential well associated with the nonzero parallel electric field in the EDR. Thus, a loss of axisymmetry in $f(V_{\perp 1}, V_{\perp 2})$ with rapidly varying

counter-streaming beam signatures and resulting parallel anisotropy of electron temperature might suggest proximity to the EDR [*Chen et al.*, 2008b; *Le et al.*, 2009, 2010; *Scudder et al.*, 2012].

[29] The 6 s gap between C1 and C4 crossing of the transition is consistent with the timing of C1/C4 crossing of the neutral sheet, across which B_x changes sign as shown in Figure 1A(a, d). (C4 observes an isotropic flat top distribution similar to Figure 4(d) at 1707:38.6 UT (not shown), ~ 6 s later than C1.) The normal separation (~ 100 km) between the two spacecraft and the 6 s gap correspond well to the normal velocity (~ 17 km/s) of the first X line that was estimated in section 2 using the repeated Hall field signatures. These indicate that the layer within/around which the electron distributions rapidly vary and/or $f(V_{\perp 1}, V_{\perp 2})$ shows a lack of axisymmetry may be parallel to the neutral sheet and moving with the first X line (or the overall reconnection current sheet structure). This enables us to set the upper bound for a thickness of the transition layer assuming that the layer is characterized by a lack of axisymmetry in $f(V_{\perp 1}, V_{\perp 2})$ observed by the spacecraft. Based on $f(V_{\perp 1}, V_{\perp 2})$ reconstructed with a 1 s shifted central time for the period of a transition layer crossing (not shown), the time period during which C4 (C1) observes the (apparent) loss of axisymmetry gives the upper bound of a thickness of 9 d_e ($3d_e$). This layer might have formed being broader away from the X line along \hat{l} , as a result, showing more gradual changes of the electron distributions with time/distance observed by C4.

[30] This observation indicates an electron-scale layer across which Cluster observed nonaxisymmetric distributions. The boundary appears to be close to the southern boundary of the O-line structure slightly below the neutral sheet (Figure 1B(e)). We note that this layer occurs in

conjunction with the fastest super-Alfvénic electron outflow jets downstream of the X line and enhanced high-energy electron fluxes (Figure 2). It is also embedded in a wider electron super-Alfvénic current layer and in the region where the Walén tests for neither the ions nor electrons are satisfied, suggesting that Cluster traversed or skimmed the tailward edge of the elongated electron current layer or the EDR. We also point out that this event differs from the reconnection event analyzed in *Chen et al.* [2008a, 2009a] where strong electron temperature anisotropy ($T_{\parallel} > T_{\perp}$) was observed in the inflow regions, whereas the electron distributions in the exhaust were nearly isotropic. The present reconnection event shows strong anisotropy in the exhaust as well as in the inflow region. The anisotropy appears to be associated with the large-scale, elongated region of electron outflowing jets. This observation is consistent with a recent numerical study by *Le et al.* [2013], who showed that the temperature anisotropy develops by electron trapping in the reconnection inflow and extends to the exhaust if the guide field is sufficiently strong that the electrons remain magnetized.

4. Conclusion

[31] We report a case study of Cluster observations of the structure, dynamics, and evolution of the reconnection site in the vicinity of reconnection X lines in the Earth's magnetotail current sheet. The consecutive flow reversals and Hall electric and magnetic geometry together with the detection of a magnetic island embedded in the outflow region indicates the existence of multiple X lines along the current sheet that was possibly unstable to the tearing mode. The plasmoid coincidentally observed during the electron super-Alfvénic outflow jets also suggests that the formation of such plasmoids results from an instability in the extended electron current layer. Comparing field and particle features between the two flow reversal periods, similarities and dissimilarities in the Hall magnetic and electric field geometry, and the enhanced energetic electron fluxes streaming along the separatrix away from the X line suggests that a second X line formed within about 20 s of the passage close to the first X line. We identified layers of a large super-Alfvénic electron outflow during the interval of a spacecraft crossing of the separatrix region and the dissipation region near the neutral sheet. While Cluster was headed toward the Southern Hemisphere and was slightly below the neutral sheet, asymmetric counter-streaming electron beams and less axisymmetric electron ($V_{\perp 1}, V_{\perp 2}$) distributions are simultaneously observed. There is an indication of electron-scale transition layer embedded in a much wider region ($20\text{--}30d_e$ thick) where the (electron) Walén test failed and the electron super-Alfvénic outflow jets and high-energy electron beams were detected. These observations of the substructure of the reconnection current sheet with similar features in the electron distributions to those predicted from PIC simulations [*Scudder and Daughton*, 2008] suggest that Cluster traversed or skimmed the tailward edge of the elongated electron current layer. We also note that this event differs from a previously reported reconnection event [*Chen et al.*, 2008a, 2009a] in that strong electron temperature anisotropy ($T_{\parallel} > T_{\perp}$) is observed both in the inflow region and in the exhaust, where the anisotropy appears to be

associated with the elongated electron outflow jets, consistent with a recent numerical study [*Le et al.*, 2013].

[32] **Acknowledgments.** We acknowledge helpful comments by J. Egedal as well as the Cluster-PEACE, FGM, CIS, EFW, and STAFF teams along with the Cluster Active Archive for providing the data used in this study. K.-J. Hwang, M. L. Goldstein, and D. E. Wendel were supported, in part, by NASA's Magnetospheric Multiscale Mission Interdisciplinary Science grant to the Goddard Space Flight Center and by the Cluster mission. C. Gurgiolo was supported, in part, by NASA grant NXX10AQ46G. A. N. Fazakerley was supported, in part, by UK STFC grant ST/H00260X/1.

[33] Philippa Browning thanks Kareem Osman and another reviewer for their assistance in evaluating this paper.

References

- Åsnes, A., M. G. G. T. Taylor, A. L. Borg, B. Lavraud, W. H. Friedel, C. P. Escoubet, H. Laasko, P. Daly, and A. N. Fazakerley (2008), Multi-spacecraft observations of electron beam in reconnection region, *J. Geophys. Res.*, **113**, A07S30, doi:10.1029/2007JA012770.
- Birn, J., et al. (2001), Geospace environmental modeling gem magnetic reconnection, *J. Geophys. Res.*, **106**, 3715–3719.
- Cai, H. J., and L. C. Lee (1997), The generalized Ohm's law in collisionless magnetic reconnection, *Phys. Plasmas*, **4**, 509.
- Chanteur, G. (1998), Spatial interpolation for four spacecraft: Theory, in *Analysis Methods for Multi-Spacecraft Data*, edited by G. Paschmann and P. W. Daly, 349 p., ESA Publications Division, Keplerlaan 1, 2200 AG Noordwijk, The Netherlands.
- Chen, L.-J., et al. (2008a), Evidence of an extended electron current sheet and its neighboring magnetic island during magnetotail reconnection, *J. Geophys. Res.*, **113**, A12213, doi:10.1029/2008JA013385.
- Chen, L. J., et al. (2008b), Evidence of an extended electron current sheet and its neighboring magnetic island during magnetotail reconnection, *J. Geophys. Res.*, **113**, A12213, doi:10.1029/2008JA013385.
- Chen, L.-J., et al. (2009a), Multi-spacecraft observations of the electron current sheet, neighboring magnetic islands, and electron acceleration during magnetotail reconnection, *Phys. Plasma*, **16**, 056501.
- Chen, L. J., et al. (2009b), Multi-spacecraft observations of the electron current sheet, neighboring magnetic islands, and electron acceleration during magnetotail reconnection, *Phys. Plasmas*, **16**, 56501.
- Coppi, B., G. Laval, and R. Pellat (1966), Dynamics of the geomagnetic tail, *Phys. Rev. Lett.*, **16**, 1207.
- Eastwood, J. P., T. D. Phan, M. Øieroset, and M. A. Shay (2010), Average properties of the magnetic reconnection ion diffusion region in the Earth's magnetotail: The 2001–2005 Cluster observations and comparison with simulations, *J. Geophys. Res.*, **115**, A08215, doi:10.1029/2009JA014962.
- Eastwood, J. P., et al. (2007), Multi-point observations of the hall electromagnetic field and secondary island formation during magnetic reconnection, *J. Geophys. Res.*, **112**, A06235, doi:10.1029/2006JA012158.
- Egedal, J., M. Øieroset, W. Fox, and R. P. Lin (2005), In situ discovery of an electrostatic potential, trapping electrons and mediating fast reconnection in the Earth's magnetotail, *Phys. Rev. Lett.*, **94**, 025006, doi:10.1029/2009JA014650.
- Egedal, J., W. Fox, M. Porkolab, M. Øieroset, R. P. Lin, W. Daughton, and J. F. Drake (2008), Evidence and theory for trapped electrons in guide field magnetotail reconnection, *J. Geophys. Res.*, **113**, A12207, doi:10.1029/2008JA013520.
- Egedal, J., A. Lê, L. J. Chen, B. Lefebvre, W. Daughton, and A. Fazakerley (2010), Cluster observation of bidirectional beams caused by electron trapping during antiparallel reconnection, *J. Geophys. Res.*, **115**, A03214, doi:10.1029/2009JA014650.
- Egedal, J., A. Le, and W. Daughton (2013), A review of pressure anisotropy caused by electron trapping in collisionless plasma, and its implications for magnetic reconnection, *Phys. Plasmas*, **20**, 18, doi:10.1063/1.4811092.
- Furth, H. P., K. Killeen, and M. N. Rosenbluth (1963), Finite-resistivity instabilities of a sheet pinch, *Phys. Fluids*, **6**, 459.
- Hesse, M. M. (2006), Dissipation in magnetic reconnection with a guide magnetic field, *Phys. Plasmas*, **13**, 122107.
- Hesse, M. M., K. Shindler, J. Birn, and M. Kuznetsova (1999), The diffusion region in collisionless magnetic reconnection, *Phys. Plasmas*, **5**, 1781.
- Hesse, M. M., M. Kuznetsova, and J. Birn (2004), The role of electron heat flux in guide-field magnetic reconnection, *Phys. Plasmas*, **11**, 5387.
- Horiuchi, R., and T. Sato (1997), Particle simulation study of collisionless driven reconnection in a sheared magnetic field, *Phys. Plasmas*, **4**, 277.
- Hoshino, M. (2005), Electron surfing acceleration in magnetic reconnection, *J. Geophys. Res.*, **110**, A10215, doi:10.1029/2005JA011229.

- Hoshino, M., T. Mukai, T. Terasawa, and I. Shinohara (2001), Superthermal electron acceleration in magnetic reconnection, *J. Geophys. Res.*, *106*, 25972.
- Karimabadi, H., W. Daughton, and J. Scudder (2007), Multi-scale structure of the electron diffusion region, *Geophys. Res. Lett.*, *34*, L13104, doi:10.1029/2007GL030306.
- Le, A., J. Egedal, W. Daughton, W. Fox, and N. Katz (2009), Equations of state for collisionless guide-field reconnection, *Phys. Rev. Lett.*, *102*, 085001.
- Le, A., J. Egedal, W. Daughton, J. F. Drake, W. Fox, and N. Katz (2010), Magnitude of the hall fields during magnetic reconnection, *Geophys. Res. Lett.*, *37*, L03106, doi:10.1029/2009GL041941.
- Le, A., J. Egedal, W. Daughton, H. Karimabadi, O. Ohia, and V. S. Lukin (2013), Regimes of the electron diffusion region in magnetic reconnection, *Phys. Rev. Lett.*, *110*, 135004.
- Mozer, F. S., S. D. Bale, J. P. McFadden, and R. B. Torbert (2005), New features of electron diffusion regions observed at subsolar magnetic field reconnection sites, *Geophys. Res. Lett.*, *32*, L24102, doi:10.1029/2005GL024092.
- Ohia, O., J. Egedal, V. S. Lukin, W. Daughton, and A. Le (2012), Demonstration of anisotropic fluid closure capturing the kinetic structure of magnetic reconnection, *Phys. Rev. Lett.*, *109*, 115004, doi:10.1103/PhysRevLett.109.115004.
- Øieroset, M., R. Lin, and T. D. Phan (2002), Evidence for electron acceleration up to similar to 300 keV in the magnetic reconnection diffusion region of Earth's magnetotail, *Phys. Rev. Lett.*, *89*(19), 195001, doi:10.1103/PhysRevLett.89.195001.
- Phan, T. D., J. F. Drake, M. A. Shay, F. S. Mozer, and J. P. Eastwood (2007), Evidence for an elongated (>60 ion skin depths) electron diffusion region during fast magnetic reconnection, *Phys. Rev. Lett.*, *99*, 225002.
- Pritchett, P. L. (2002), Geospace environment modeling magnetic reconnection challenge: Simulations with a full particle electromagnetic code, *J. Geophys. Res.*, *107*, 1402, doi:10.1029/2001JA009149.
- Ricci, P., G. Lapenta, and J. U. Brackbill (2002), Gem reconnection challenge: Implicit kinetic simulations with the physical mass ratio, *Geophys. Res. Lett.*, *29*(23), 2088, doi:10.1029/2002GL015314.
- Scudder, J. D., and W. Daughton (2008), "Illuminating" electron diffusion regions of collisionless magnetic reconnection using electron agyrotropy, *J. Geophys. Res.*, *113*, A06222, doi:10.1029/2008JA013035.
- Scudder, J. D., P. A. Puhl-Quinn, F. S. Mozer, K. W. Ogilvie, and C. T. Russell (1999), Generalized Walén tests through Alfvén waves and rotational discontinuities using electron flow velocities, *J. Geophys. Res.*, *104*, 19,817–19,834, doi:10.1029/1999JA900146.
- Scudder, J. D., F. S. Mozer, N. C. Maynard, and C. T. Russell (2002), Fingerprints of collisionless reconnection at the separator, I. Ambipolar-Hall signatures, *J. Geophys. Res.*, *107*(A10), 1294, doi:10.1029/2001JA000126.
- Scudder, J. D., R. D. Holdaway, W. S. Daughton, H. Karimabadi, V. Roytershteyn, C. T. Russell, and J. Y. Lopez (2012), First resolved observation of the demagnetized electron-diffusion region of an astrophysical magnetic-reconnection site, *Phys. Rev. Lett.*, *108*, 225005-1, doi:10.1103/PhysRevLett.108.225005.
- Shay, M. A., J. F. Drake, and B. N. Rogers (1999), The scaling of collisionless, magnetic reconnection for large systems, *Geophys. Res. Lett.*, *26*, 2163.
- Shay, M. A., J. F. Drake, and M. Swisdak (2007), Two-scale structure of the electron dissipation region during collisionless magnetic reconnection, *Phys. Rev. Lett.*, *99*, 155002.
- Vaivads, A. A., A. Retinò, and M. André (2006), Microphysics of magnetic reconnection, *Space Sci. Rev.*, *122*, 19.
- Wang, R., Q. Lu, A. Du, and S. Wang (2011), In Situ observations of a secondary magnetic island in an ion diffusion region and associated energetic electrons, *Phys. Rev. Lett.*, *104*, 175003.
- Wendel, D. E., and P. H. Reiff (2009), Magnetic reconnection impact parameters from multiple spacecraft magnetic field measurements, *Geophys. Res. Lett.*, *36*, L20108, doi:10.1029/2009GL040228.
- Wygant, J. R., et al. (2005), Cluster observations of an intense normal component of the electric field at a thin reconnecting current sheet in the tail and its role in the shock-like acceleration of the ion fluid into the separatrix region, *J. Geophys. Res.*, *110*, A09206, doi:10.1029/2004JA010708.